Eur. Phys. J. B (2014) 87: 124
DOI: 10.1140/epjb/e2014-50076-6

THE EUROPEAN PHYSICAL JOURNAL B

Regular Article

Spin-orbit effects in carbon nanotubes – Analytical results

Konstantin Nikolaevich Pichugin[1], Mihal Pudlak[2], and Rashid Giyasovich Nazmitdinov[3,4,a]

[1] Kirensky Institute of Physics, 660036 Krasnoyarsk, Russia
[2] Institute of Experimental Physics, Watsonova 47, 04001 Košice, Slovak Republic
[3] Departament de Física, Universitat de les Illes Balears, 07122 Palma de Mallorca, Spain
[4] Bogoliubov Laboratory of Theoretical Physics, Joint Institute for Nuclear Research, 141980 Dubna, Russia

Received 3 February 2014 / Received in final form 26 March 2014
Published online 2 June 2014 –

Abstract. Energy spectra and transport properties of armchair nanotubes with curvature induced spin-orbit interaction are investigated thoroughly. The spin-orbit interaction consists of two terms: the first one preserves the spin symmetry in rotating frame, while the second one breaks it. It is found that the both terms are equally important: (i) at scattering on the potential step which mimics a long-range potential in the nanotubes; (ii) at transport via nanotube quantum dots. It is shown that an armchair nanotube with the first spin-orbit term works as an ideal spin-filter, while the second term produces a parasitic inductance.

1 Introduction

Electronic and transport properties of carbon nanotubes are highly topical subjects in mesoscopic physics (see for a review [1–4]) due to potential technological applications in nano-electronics and optical devices [5,6]. Among various studies of physical properties of carbon nanotubes (CNTs), a detailed understanding of spin-orbit interaction is crucial for the interpretation of ongoing experiments, as well as for future applications of the nanotubes in spintronics.

In general, the intrinsic (intraatomic) spin-orbit interaction in graphene is weak [7], since carbon atoms have zero nuclear spins, and the hyperfine interaction of electron spins with nuclear spins is suppressed. It makes a spin decoherence in such material to be weak as well, i.e., scattering due to disorder is supposed to be not important. A full analysis of spin-orbit interaction in CNTs requires, however, to consider the isospin degree of freedom present in the honeycomb carbon lattice.

According to a general wisdom, graphene being a zero-gap semiconductor has a band structure described by a linear dispersion relation at low energy, similar to massless Dirac-Weyl fermions [1,8]. For a CNT the quantization condition leads, however, to metallic or semiconducting behavior, depending on chirality [2,3]. The curved geometry may give rise to a band gap even for metallic CNTs [9]. Such a gap would allow to confine electrons, otherwise not possible due to the Klein paradox [10]. However, a precise form of the spin-orbit interaction in a single-layer graphene nanotube is still not well known.

A consistent approach to introduce the curvature-induced spin-orbit coupling (SOC) in the low-energy physics of graphene have been developed by Ando [11] and by others [12–14]. Recent measurements in ultra clean CNTs [15], at various values of the magnetic field, revealed the energy splitting which can be associated with a spin-orbit coupling. Indeed, the measured shifts are compatible with theoretical predictions [11,14]. However, some features are left debatable. Evidently, removing the degeneracy between quantum levels, the magnetic field generates new mechanisms as well, which obscure effects related to a plain spin-orbit coupling (see, for example, discussion in [16–20]).

It is noteworthy on the pivotal fact that within the approach developed by Ando [11] one obtains two SOC terms: one preserves the spin symmetry in the rotating frame (see below), while the second one breaks this symmetry. In previous studies [11,14] the role played by the second term was underestimated. The purpose of the present paper is twofold. First, to consider consistently a full curvature-induced spin-orbit coupling in an armchair nanotube within the approach suggested by Ando [11]. Second, to show that the second term could play an important role in transport phenomena. In order to illuminate the role of interplay between both terms on electron transport, we analyze the situation at zero magnetic field, removing all additional mechanisms related to the magnetic field. In contrast to previous studies, we also provide analytical estimations for the energy spectrum and transport coefficients for different cases (with and without the second term). Evidently, the analytical approach gives a fundamental insight into the nature of electronic and transport properties of CNTs.

The structure of the paper is as follows. In Section 2 we derive an explicit formula for eigen spectrum of the Ando Hamiltonian with a full curvature-induced

[a] e-mail: rashid@theor.jinr.ru

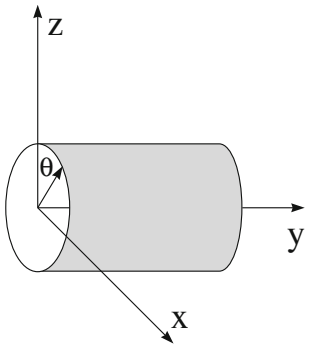

Fig. 1. The coordinate system for the carbon nanotube.

spin-orbit coupling in a CNT. In Section 3 we discuss different symmetries associated with the Hamiltonian and analyze the current operators. Section 4 is devoted to the analysis of scattering phenomena at the interface introduced by a potential step and to transport properties of carbon quantum dots at the preserved spin symmetry. In Section 5, with the aid of results of Section 6, we discuss transport effects produced by a full curvature-induced spin-orbit coupling in an armchair nanotube. Main conclusions are summarized in Section 7. Appendix provides technical details used for analytical solutions.

2 The model

Figure 1 sketches a carbon nanotube and a coordinate system with respect to the orientation axis of a carbon nanotube in our analysis. The orbitals corresponding to the σ bands of graphene are made by linear combinations of the $2s$, $2p_x$, $2p_y$ atomic orbitals, whereas the orbitals of the π band are p_z orbitals.

Starting from the tight-binding model, with the aid of $\mathbf{k}\cdot\mathbf{p}$ scheme in the vicinity of the Fermi energy ($E=0$) at K and K' points of the first Brillouin Zone, Ando has derived the effective mass Hamiltonian for electrons on curved surface with spin-orbit interaction (see details in [11]). We follow this approach and use the effective mass Hamiltonian as a starting point of our analysis. This Hamiltonian can be expressed in the form of matrix-Hamiltonian equation

$$\hat{H}\Psi = \begin{pmatrix} 0 & \hat{f} \\ \hat{f}^\dagger & 0 \end{pmatrix} \begin{pmatrix} F_A^K \\ F_B^K \end{pmatrix} = E \begin{pmatrix} F_A^K \\ F_B^K \end{pmatrix}, \tag{1}$$

with the following definitions

$$\begin{aligned} \hat{f} &= \gamma\left(\hat{k}_x - i\hat{k}_y\right) + i\frac{\delta\gamma'}{4R}\hat{\sigma}_x(\boldsymbol{r}) - \frac{2\delta\gamma p}{R}\hat{\sigma}_y, \\ \hat{k}_x &= -i\frac{\partial}{R\partial\theta}, \hat{k}_y = -i\frac{\partial}{\partial y}, \\ \hat{\sigma}_x(\boldsymbol{r}) &= \hat{\sigma}_x\cos\theta - \hat{\sigma}_z\sin\theta. \end{aligned} \tag{2}$$

Here, $\hat{\sigma}_{x,y,z}$ are standard Pauli matrices, and the spinors of two sub-lattices are

$$F_A^K = \begin{pmatrix} F_{A,\uparrow}^K \\ F_{A,\downarrow}^K \end{pmatrix}, \quad F_B^K = \begin{pmatrix} F_{B,\uparrow}^K \\ F_{B,\downarrow}^K \end{pmatrix}. \tag{3}$$

We preserve the definitions introduced by Ando [11] for the following parameters:

$$\begin{aligned} \gamma &= -\sqrt{3}V_{pp}^\pi a/2, \\ \gamma' &= \sqrt{3}\left(V_{pp}^\sigma - V_{pp}^\pi\right)a/2, \\ p &= 1 - 3\gamma'/8\gamma. \end{aligned} \tag{4}$$

Here, the quantities V_{pp}^σ and V_{pp}^π are the transfer integrals for σ and π orbitals, respectively in a flat 2D graphene, and a is a lattice constant ($a = 2.46$ Å). The intrinsic source of the SOC $\delta = \Delta/(3\epsilon_{\pi\sigma})$ is defined by:

$$\Delta = i\frac{3\hbar}{4m_e^2c^2}\left\langle x_l\left|\frac{\partial V}{\partial x}\hat{p}_y - \frac{\partial V}{\partial y}\hat{p}_x\right|y_l\right\rangle \tag{5}$$

and $\epsilon_{\pi\sigma} = \epsilon_{2p}^\pi - \epsilon_{2p}^\sigma$, where V is the atomic potential. The energy ϵ_{2p}^σ is the energy of σ-orbitals which are localized between carbon atoms. The energy ϵ_{2p}^π is the energy of π-orbitals which are directed perpendicular to the nanotube surface. In our consideration x_l, y_l, and z_l are local coordinates; z_l-axis is perpendicular to a graphene plane, and y_l-axis is lying along the tube symmetry axis.

Ando suggested to neglect a spin-orbit term proportional to σ_x, i.e., the term $\delta\gamma'/(4R)\hat{\sigma}_x(\boldsymbol{r})$ in the Hamiltonian (1). He assumed that a spin projection on the CNT symmetry axis (y-axis) is a conserved integral of motion. Based on the perturbative approach result, he concluded that a spin mixing in the wave function due to this term is very small. Ando admitted, however, that it may couple states from bands with different spin quantum numbers and lead to a small spin relaxation. Although in reference [19] a different basis was used to derive the effective Hamiltonian for a single wall CNT, the term breaking its spin symmetry (a conservation of $\hat{s}_z$-component) was obtained as well. Similar to reference [11], it was also suggested in reference [19] to neglect such a term. In contrast, we consider all spin-orbit terms on equal footing, since even a small perturbation brought about by the second term breaks the fundamental spin symmetry of the total Hamiltonian. In this case all three spin projections are not conserved in any system. Different bands must be distinguished by the magnetic quantum number m which is a projection of the total angular momentum on the symmetry axis of the CNT (see below). As a result, this preserved fundamental symmetry allows to couple states with different spins even inside one band. We restrict our consideration by an armchair CNT. In this case the electron-hole asymmetry observed in the experiment [15] at zero magnetic field is absent [19,20].

To get rid of the θ dependence in the Hamiltonian (1), we apply the transformation

$$\hat{H}' = \hat{U}\hat{H}\hat{U}^{-1} \tag{6}$$

with the aid of the unitary operator $\hat{U}$

$$\hat{U} = \begin{pmatrix} \exp(i\frac{\theta}{2}\hat{\sigma}_y) & 0 \\ 0 & \exp(i\frac{\theta}{2}\hat{\sigma}_y) \end{pmatrix}. \tag{7}$$

As a result, we obtain the Hamiltonian in the transformed frame

$$\hat{H}' = \hat{H}_{kin} + \hat{H}_{SOC}, \tag{8}$$

$$\hat{H}_{kin} = -i\gamma\left(\hat{\tau}_y \otimes I\partial_y + \hat{\tau}_x \otimes I\frac{1}{R}\partial_\theta\right), \tag{9}$$

$$\hat{H}_{SOC} = -\lambda_y\hat{\tau}_y \otimes \hat{\sigma}_x - \lambda_x\hat{\tau}_x \otimes \hat{\sigma}_y, \tag{10}$$

where I is 2×2 unity matrix, and

$$\lambda_x = \gamma\left(1 + 4\delta p\right)/(2R), \quad \lambda_y = \delta\gamma'/(4R). \tag{11}$$

We distinguish in the Hamiltonian (8) the kinetic $\hat{H}_{kin}$ and the potential $\hat{H}_{SOC}$ terms. Here, the operators $\hat{\tau}_{x,y,z}$ are the Pauli matrices which act on the wave functions of A- and B-sub-lattices (a pseudo-spin space). Note that the kinetic term couples the wave functions of A- and B-sub-lattices, as well as the potential term.

In our consideration, the curvature-induced spin-orbit coupling is described by two terms: λ_x and λ_y. The term λ_x depends on: (i) values of the transfer integral V_{pp}^{π} for π orbitals; and (ii) combined action produced by a product of the *intrinsic* spin-orbit interaction and the difference between the transfer integrals V_{pp}^{π}, V_{pp}^{σ} for π and σ orbitals, respectively, in a flat 2D graphene. The term λ_y depends on the difference between the transfer integrals V_{pp}^{π}, V_{pp}^{σ} for π and σ orbitals, respectively, in a flat 2D graphene. Both terms are inversely proportional to the tube radius, and tend to zero at $R \to \infty$, i.e., in the limit of a flat graphene. For small nanotubes (small radius) we might expect, however, that effects produced by these terms come into particular prominence in transport phenomena.

Herewith, for the sake of convenience, we use $\hbar = 1$, if otherwise it will be not mentioned. At $\lambda_y = 0$, the spin projection $\hat{S}_y = \frac{1}{2}I \otimes \hat{\sigma}_y$ is a constant of motion, since it commutes with the Hamiltonian $[\hat{S}_y, \hat{H}'] = 0$. The term $\lambda_y \neq 0$ breaks this symmetry and yields a spin mixing. Due to an axial symmetry of the CNT, the projection of a total angular momentum on the nanotube symmetry axis is always the integral of motion. In our consideration, in the transformed system the integral of motion $\hat{J}_y$

$$\hat{J}_y = I \otimes \left(\hat{L}_y + \frac{\hat{\sigma}_y}{2}\right) = I \otimes \left(-i\partial_\theta + \frac{\hat{\sigma}_y}{2}\right), \left[\hat{H}, \hat{J}_y\right] = 0 \tag{12}$$

takes a simple form

$$\hat{J}_y \to \hat{J}'_y = \hat{U}\hat{J}_y\hat{U}^{-1} = I \otimes (-i\partial_\theta). \tag{13}$$

In virtue of this fact, we consider the wave function in the form of plane waves

$$F'(\theta, y) = e^{im\theta}e^{ik_y y}\Psi, \tag{14}$$

where the wave function Ψ is a four-component spinor. The wave function (14) defines the eigenvalues m of the operator $\hat{J}'_y$

$$\hat{J}'_y F'(\theta, y) = mF'(\theta, y), \; m = \pm 1/2, \pm 3/2, \ldots, \tag{15}$$

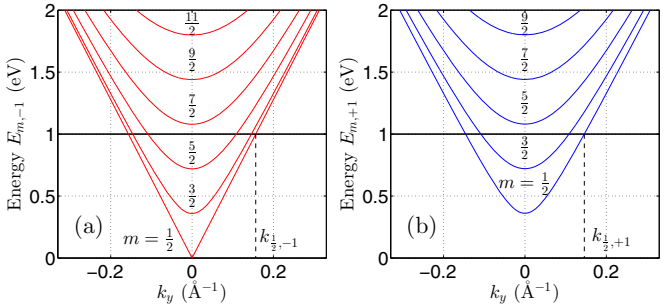

Fig. 2. Positive spectrum (see Eqs. (A.4)) $E_{m,\ 1}$ (a) and $E_{m,+1}$ (b) as a function of the wave number k_y. The values of $k_{m,+1}$ and $k_{m,\ 1}$ for $m = 1/2$ at the energy $E_F = 1$ eV (solid horizontal line) are indicated by vertical dashed lines. The parameters are $R = 17.75$ Å, $\delta = 0.01$, $p = 0.1$, $\gamma = \frac{9}{2}1.42$ Å eV, $\gamma\ = \gamma\frac{8}{3}$, $\lambda_x = \frac{\gamma}{R}(1/2 + 2\delta p) = 0.18$ eV, $\lambda_y = \frac{\delta\gamma'}{4R} = 0.0024$ eV.

while a quantum number k_y is an eigenvalue of the operator $\hat{k}'_y \equiv \hat{k}_y$

$$\hat{k}'_y F'(\theta, y) = k_y F'(\theta, y). \tag{16}$$

Taking into account equations (8) and (14), we obtain our Hamiltonian

$$\hat{H}'(m, k_y) = \begin{pmatrix} 0 & 0 & t_m - it_y & i(\lambda_y + \lambda_x) \\ 0 & 0 & i(\lambda_y - \lambda_x) & t_m - it_y \\ t_m + it_y & -i(\lambda_y - \lambda_x) & 0 & 0 \\ -i(\lambda_y + \lambda_x) & t_m + it_y & 0 & 0 \end{pmatrix}, \tag{17}$$

which acts on the spinor Ψ. Here we introduce the following definitions:

$$t_m = \frac{\gamma}{R}m, \; t_y = \gamma k_y. \tag{18}$$

The solution of the eigenvalue problem of Hamiltonian (17) yields the following four energies (see Appendix, Eqs. (A.4))

$$E^{(+)} = +E_{m,s}, E^{(-)} = -E_{m,s}, \quad s = \pm 1. \tag{19}$$

We define all states with $E^{(+)} > 0$ ($E^{(-)} < 0$) as a particle (hole) states. As was mentioned above, there is the electron-hole symmetry $|E^{(+)}| = |E^{(-)}|$.

The energy spectrum for a typical CNT as a function of the continuous variable k_y and the quantized projection of the angular momentum m is shown on Figure 2. For the sake of illustrations, in numerical calculations we use the following parameters [11]: $V_{pp}^{\pi} \sim -3$ eV, $V_{pp}^{\sigma} \sim 5$ eV, $|p| \sim 0.1$, the bond length $d = a/\sqrt{3} \approx 1.42$ Å. For a given m-value the Fermi energy E_F provides four possible values for k_y: $\pm k_{m,s}$.

The energy gap $\Delta E_{m,s}$ in the CNT is defined by a minimal distance between negative and positive parts of

the spectrum (see Eqs. (A.4))

$$\Delta E_{m,s}=2|E_{m,s}(k_y=0)|=2\left|\sqrt{t_m^2+\lambda_y^2}+s\lambda_x\right|\equiv 2E^0_{m,s}. \tag{20}$$

At $\lambda_y=0$ there is a minimal gap $\Delta E_{1/2,-1}=4\gamma\delta|p|/R$, which coincides with the value obtained by Ando [11]. At $\lambda_x\neq 0$ and $\lambda_y\neq 0$ for $p>0$ the minimal gap becomes even lesser, while for $p<0$ it increases. Thus, the comparison of the gap (20) with experimental data would allow to fix the model parameters (4). The transport does not persist in the gap, since all eigen modes are evanescent ones. Evidently, when the spin-orbit interaction ($\delta=0$) is zero, one is faced with a plain metallic CNT.

3 Symmetries and current operators

The Hamiltonian (8) has several symmetries. There is a particle-hole symmetry

$$\hat{M}_a\hat{H}'\hat{M}_a^{-1}=-\hat{H}', \tag{21}$$

defined by the operator

$$\hat{M}_a=\hat{\tau}_z\otimes I. \tag{22}$$

Therefore, energies for the eigenfunctions Ψ and $\hat{M}_a\Psi$ are equal in value but opposite in sign. There are two inversion operators M_θ, M_y, for θ, y coordinates, respectively,

$$\hat{M}_y=\hat{\tau}_y\otimes\hat{\sigma}_y,\quad \hat{M}_\theta=\hat{\tau}_y\otimes\hat{\sigma}_x, \tag{23}$$

with properties

$$\hat{M}_y\hat{H}'(\hat{k}_y,\hat{J}_y)\hat{M}_y^{-1}=\hat{H}'(-\hat{k}_y,\hat{J}_y), \tag{24}$$

$$\hat{M}_\theta\hat{H}'(\hat{k}_y,\hat{J}_y)\hat{M}_\theta^{-1}=\hat{H}'(\hat{k}_y,-\hat{J}_y). \tag{25}$$

These transformations connect the eigenfunctions with opposite quantum numbers k_y and m.

In virtue of the conservation law for the current $\mathbf{j}=\mathbf{j_y}+\mathbf{j}_\theta$

$$\frac{\partial}{\partial t}|\Psi|^2+\nabla\mathbf{j}=0, \tag{26}$$

we obtain a longitudinal and an orbital current operators

$$\hat{j}_y=\gamma\hat{\tau}_y\otimes I,\quad \hat{j}_\theta=\gamma\hat{\tau}_x\otimes I. \tag{27}$$

The same expressions can be obtained from the equation of motion

$$\hat{v}=\dot{\hat{r}}=i\left[\hat{H}',\hat{r}\right]. \tag{28}$$

For fixed quantum numbers (k_y,m), at $E>0$ the current moves in a direction opposite to one of the current at $E<0$. This fact follows from the symmetry relation

$$\hat{M}_a^{-1}\hat{j}_{y,\theta}\hat{M}_a=-\hat{j}_{y,\theta}. \tag{29}$$

The expectation values of the θ (y)-component of the current calculated by means of the eigenfunctions Ψ and $M_\theta\Psi$ ($M_y\Psi$) are of opposite sign. This result follows from the following identities:

$$\hat{M}_\theta^{-1}\hat{j}_\theta\hat{M}_\theta=-\hat{j}_\theta,\quad \hat{M}_y^{-1}\hat{j}_\theta\hat{M}_y=\hat{j}_\theta, \tag{30}$$

$$\hat{M}_\theta^{-1}\hat{j}_y\hat{M}_\theta=\hat{j}_y,\quad \hat{M}_y^{-1}\hat{j}_y\hat{M}_y=-\hat{j}_y. \tag{31}$$

With the aid of the relations

$$\hat{M}_\theta^{-1}\hat{S}_{y,z}\hat{M}_\theta=-\hat{S}_{y,z}, \tag{32}$$

$$\hat{M}_\theta^{-1}\hat{S}_x\hat{M}_\theta=\hat{S}_x, \tag{33}$$

$$\hat{M}_y^{-1}\hat{S}_{x,z}\hat{M}_y=-\hat{S}_{x,z}, \tag{34}$$

$$\hat{M}_y^{-1}\hat{S}_y\hat{M}_y=\hat{S}_y, \tag{35}$$

it could be shown that the expectation values of spin projections onto the local y,z (x,z)-axes for the eigenfunctions Ψ and $M_\theta\Psi$ ($M_y\Psi$) have also opposite signs.

4 Analytical results at $\lambda_y=0$

To understand how the full SOC affects the system properties, we consider first only $\lambda_x\neq 0$, $\lambda_y=0$. As discussed above, in this case the operator $\hat{S}_y=\frac{1}{2}I\otimes\hat{\sigma}_y$ is an integral of motion. Therefore, we transform our Hamiltonian to the frame where the operator $\hat{S}_y$ has a diagonal form

$$\hat{\mathcal{V}}^{-1}\hat{S}_y\hat{\mathcal{V}}=\frac{1}{2}\hat{\sigma}_z\otimes I. \tag{36}$$

Here, the transformation $\hat{\mathcal{V}}$, defined as:

$$\hat{\mathcal{V}}=\left(\exp\left(i\frac{\pi}{4}\hat{\sigma}_x\right)\otimes I\right)\hat{P}_{23},\hat{P}_{23}=\begin{pmatrix}1&0&0&0\\0&0&1&0\\0&1&0&0\\0&0&0&1\end{pmatrix}, \tag{37}$$

consists of a rotation on angle $\pi/2$ around x-axis and the permutation P_{23}. This permutation collects spin up components of the A- and B-sub-lattices in the upper part of the spinor Ψ. In virtue of this transformation, the Hamiltonian (17) gains a block-diagonal structure

$$\hat{\mathcal{H}}=\hat{\mathcal{V}}^{-1}\hat{H}'\hat{\mathcal{V}}=\begin{pmatrix}0&a_-&0&0\\a_+&0&0&0\\0&0&0&b_-\\0&0&b_+&0\end{pmatrix}, \tag{38}$$

$$a_\pm=(t_m-\lambda_x)\pm it_y,\quad b_\pm=(t_m+\lambda_x)\pm it_y.$$

One obtains obvious four eigenvalues and eigenvectors

$$E^{(\pm)}=\pm E_{m,s},\quad E_{m,s}=\sqrt{(t_m+s\lambda_x)^2+t_y^2}, \tag{39}$$

$$V_{m,+1}=\frac{1}{\sqrt{2}}\left(0,0,1,z_{m,+1}\right)^T, \tag{40}$$

$$V_{m,-1}=\frac{1}{\sqrt{2}}\left(1,z_{m,-1},0,0\right)^T, \tag{41}$$

$$z_{m,s}=\left((t_m+s\lambda_x)+it_y\right)/E. \tag{42}$$

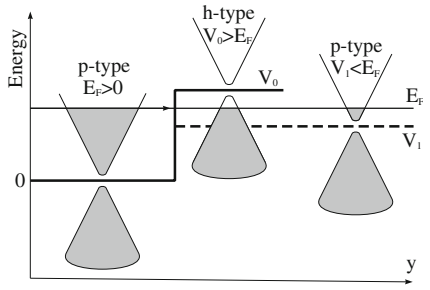

Fig. 3. A schematic illustration of the scattering process on a potential step.

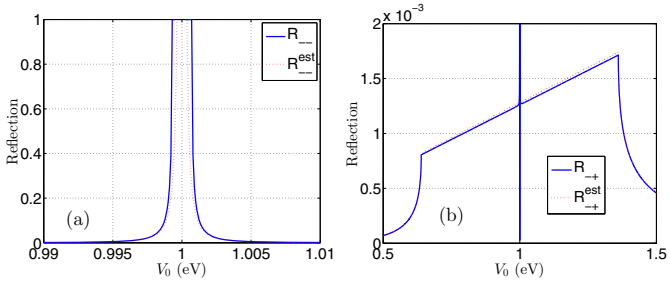

Fig. 4. Reflection probabilities on the potential step for the state $m = 1/2$, $s = -1$: analytical estimation (dotted line, red) and numerical results (solid line, blue) as a function of the potential height V_0. (a) $\lambda_y = 0$: a direct reflection $R^{\rm est}(V_0) = |r^{m,s}_{m,s}(V_0)|^2$ is described by equation (47); (b) $\lambda_y \neq 0$: a spin-flip reflection $R^{\rm est}_{+}(V_0) = |r^{m,s}_{m,\ s}(V_0)|^2$ is described by equation (66). $E_F = 1$ eV and the other parameters are the same as in Figure 2.

4.1 Scattering on a potential step

We consider first the scattering at the interface introduced by a potential step of the height V_0 as sketched in Figure 3. On the one hand, the step is assumed to be smooth on the length scale of a graphene unit cell (an inverse Brillouin momentum $2\pi/K$) and, therefore, does not induce the intervalley ($K \to K'$) scattering. On the other hand, it is assumed to be sharp on the Fermi length scale ($\lambda \sim 1/k_F$). Since θ and y are independent variables, such a potential conserves the angular momentum projection m.

Depending on the sign of E_F (incoming particle) and the sign of $E_F - V_0$ (outgoing particle) there are four types of transmission through the step: p-p, p-h, h-p, h-h. We denote particle by symbol "p", while a hole by a symbol "h". For the sake of illustration, p-p and p-h transmissions are schematically shown on Figure 3.

Transmission (reflection) of electrons incoming from the left is controlled by partial coefficients. Namely, we have $|t^q_{q'}|^2 (|r^q_{q'}|^2)$ describing transmission (reflection) probability from the left states with a set of quantum numbers $q = \{m, s\}$ to the right states with $q' = \{m', s'\}$. Transmission (reflection) probabilities are defined as squares of the scattering-wave-function amplitudes which satisfy the continuity of wave functions. Evidently, since spin is a good quantum number as well as a quantum number m, the transmission (reflection) probabilities, responsible for the spin-flip process, are absent at $\lambda_y = 0$: $|t^{m,s}_{m,s'}|^2 = |r^{m,s}_{m,s'}|^2 = 0$ for $s \neq s'$.

Matching the eigenfunctions with the same values of the angular momentum and spin projections on the left and right sides of the potential step, we obtain the following equation:

$$\frac{\left[\begin{pmatrix}1\\ Z_q\end{pmatrix} + r^q_q \begin{pmatrix}1\\ Z_q^{-1}\end{pmatrix}\right]}{\sqrt{|\gamma i(z_q^* - z_q)|}} = \frac{t^q_q}{\sqrt{|\gamma i(\tilde{z}_q^* - \tilde{z}_q)|}} \begin{pmatrix}1\\ \tilde{Z}_q\end{pmatrix}. \quad (43)$$

Here $Z_q = (z_q)^{\mathrm{sign}(E_F)}$ ($\tilde{Z}_q = (\tilde{z}_q)^{\mathrm{sign}(E_F - V_0)}$) are defined by equation (42), z_q^* ($\tilde{z}_q^*$) are complex conjugate, and the energy $E = E_F$ ($E = E_F - V_0$) before (after) the step. The wave functions are normalized to have a unit current flow along the y-axis. The solution of equation (43) defines the reflection and transmission coefficients

$$r^q_q = (Z_q - \tilde{Z}_q)/(\tilde{Z}_q - Z_q^{-1}), \quad (44)$$

$$t^q_q = (Z_q - Z_q^{-1})/(\tilde{Z}_q - Z_q^{-1}) \sqrt{\left|\frac{\tilde{z}_q - \tilde{z}_q^*}{z_q - z_q^*}\right|}. \quad (45)$$

In order to reveal the effect of the SOC let us consider the case of quantum numbers $q_n : \{m = \mp\frac{1}{2}, s = \pm 1\}$. It corresponds to a normal incident direction of electrons on the potential step for the CNT without the SOC and $\delta = 0$. Note that the variable z_q ($\tilde{z}_q$) (see Eq. (42)) depends on the term $t_m + s\lambda_x$. In our case this term transforms to the form

$$t_m + s\lambda_x = \frac{\gamma}{R}(m + s/2 + 2sp\delta) \Rightarrow \pm\frac{\gamma}{R} 2p\delta, \quad (46)$$

which depends on a small parameter δ. The Taylor series expansion of the reflection $r^{q_n}_{q_n}$ (see Eq. (44)) over this parameter δ enables to us to define the first nonzero term (omitting unimportant phase factor)

$$r^{q_n}_{q_n} = \delta p \frac{\gamma}{R} \frac{V_0}{E_F(E_F - V_0)} + O(\delta^2). \quad (47)$$

The estimation (47) describes remarkably well numerical results for the scattering until E_F or $E_F - V_0$ is close to the gap (see Fig. 4a). Thus, at $|E_F| \gg E^0_{q_n}$ and $|E_F - V_0| \gg E^0_{q_n}$, where $E^0_{q_n} = 2|\delta p\gamma|/R$ is of order 10^{-4} eV for the typical parameters of CNTs, there is a weak backward scattering defined by equation (47).

To gain a better insight into scattering phenomena we study the current. At $\lambda_y = 0$ the expectation value of the longitudinal current $\langle\hat{j}_y\rangle$ is determined by the quantum number k_y. The effect of the SOC is visible in the expectation value of the orbital (θ-) component of the current (see Appendix, Eq. (A.7))

$$\langle\hat{j}_\theta\rangle_q = \frac{\gamma}{E}(t_m + s\lambda_x), \quad (48)$$

which depends on the spin-orbit term λ_x. With the aid of equations (11) and (18), one obtains that the orbital

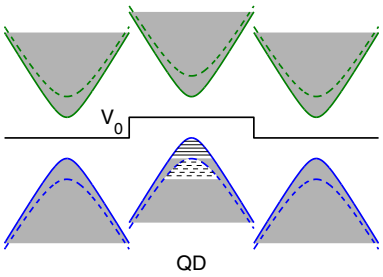

Fig. 5. A schematic picture of quantum dot in CNT. Dashed lines correspond to different sets of conserved quantum numbers.

current is always nonzero. Thus, we can have a persistent current without a magnetic field. In order to understand this result let us assume that there is a magnetic field along the symmetry axis y. It results in the Aharonov-Bohm magnetic flux passing through the CNT cross section, which yields the modified quantum number $m' = m + \phi/\phi_0$ (ϕ – magnetic flux, ϕ_0 – magnetic flux quanta). Evidently, with the aid of the magnetic field along the symmetry axis y one can suppress the orbital current for any value of the quantum number m (without the Zeeman splitting). Taking into account equations (11), (18) and (48), we obtain the condition for a zero orbital current for a magnetic quantum number m

$$t_{m'} = -s\lambda_x \Rightarrow \phi/\phi_0 = -\left(\frac{s}{2} + m\right) - 2s\delta p. \tag{49}$$

In particular, for the set of quantum numbers $q_n = \{m = \mp\frac{1}{2}, s = \pm 1\}$ we obtain $\langle\hat{j}_\theta\rangle_q = 0$ at the magnetic flux $\phi/\phi_0 = -2s\delta p$ which compensates the SOC term λ_x at $m = -1/2$. Note that at the condition (49) (and $\lambda_y = 0$) the gap (20) vanishes as well for any m.

Thus, the SOC works as an "effective magnetic field", responsible for the orbital motion and, therefore, for the weak backward scattering (47). In the absence of Zeeman splitting the applied magnetic field $\phi/\phi_0 = -2s\delta p$ leads to zero backward scattering in all orders.

4.2 Quantum dot

The gap in CNTs (due to the SOC) opens a possibility to create a nanotube quantum dot (QD), by confining particles in a quantum well with a potential $V_0(\theta(y)-\theta(L-y))$ (where $\theta(x)$ is a Heaviside step functions), as illustrated in Figure 5. We recall that in the gap there are evanescent modes only.

The QD energies are located within the gap $-E_q^0 < E < E_q^0$ (see Eq. (20)). Different sets of quantum numbers $q = \{m, s\}$ determine the full spectrum of the QD. Matching the eigenfunctions (40) at the $y = 0$ and $y = L$ we obtain the following equations:

$$r_l \begin{pmatrix} 1 \\ z_q^{-1} \end{pmatrix} = a \begin{pmatrix} 1 \\ \tilde{z}_q \end{pmatrix} + b \begin{pmatrix} 1 \\ \tilde{z}_q^{-1} \end{pmatrix}, \tag{50}$$

$$r_r \begin{pmatrix} 1 \\ z_q \end{pmatrix} = a e^{ik_q(E)L} \begin{pmatrix} 1 \\ \tilde{z}_q \end{pmatrix} + b e^{-ik_q(E)L} \begin{pmatrix} 1 \\ \tilde{z}_q^{-1} \end{pmatrix}, \tag{51}$$

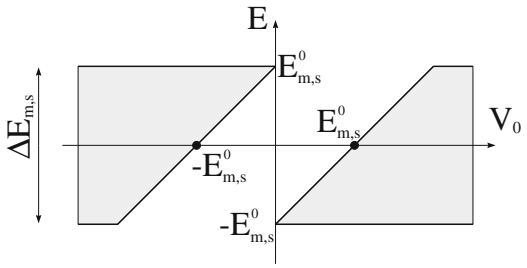

Fig. 6. Grey regions correspond to the area where discrete spectrum is possible.

where

$$\begin{aligned} z_q(E) &= \left[(t_m + s\lambda_x) - \kappa_q(E)\gamma\right]/E, \\ \kappa_q(E) &= \sqrt{(t_m + s\lambda_x)^2 - E^2}/\gamma, \\ \tilde{z}_q(E) &= \left[(t_m + s\lambda_x) + ik_q(E)\gamma\right]/(E - V_0), \\ k_q(E) &= \sqrt{(E - V_0)^2 - (t_m + s\lambda_x)^2}/\gamma. \end{aligned} \tag{52}$$

These equations could be written in the matrix form

$$\begin{pmatrix} -1 & 1 & 1 & 0 \\ -z_q^{-1} & \tilde{z}_q & \tilde{z}_q^{-1} & 0 \\ 0 & e^{ik_q(E)L} & e^{-ik_q(E)L} & -1 \\ 0 & \tilde{z}_q e^{ik_q(E)L} & \tilde{z}_q^{-1} e^{-ik_q(E)L} & -z_q \end{pmatrix} \begin{pmatrix} r_l \\ a \\ b \\ r_r \end{pmatrix} = 0. \tag{53}$$

Evidently, the solutions exist, if the determinant of equation (53) is zero. This requirement yields the transcendental equation which defines the eigen spectrum E_q^n of the QD:

$$\exp\left(2ik_q(E_q^n)L\right) = \left(\frac{z_q(E_q^n)\tilde{z}_q(E_q^n) - 1}{z_q(E_q^n) - \tilde{z}_q(E_q^n)}\right)^2, \quad n = 1, 2, 3\ldots \tag{54}$$

Equation (54) can be transformed to the form

$$\tan(k_q(E_q^n)L) = \left(\frac{\gamma^2 k_q(E_q^n)\kappa_q(E_q^n)}{E_q^n(E_q^n - V_0) - (t_m + s\lambda_x)^2}\right). \tag{55}$$

As it was mentioned above, the QD spectrum is defined in the energy window $-E_q^0 < E_q^n < E_q^0$. Its boundaries are shown on Figure 6. Thus, equation (55) corresponds to the case $\lambda_y = 0$, when there is no spin scattering. In other words, in such QDs electron with spin up cannot scattered into state with spin down and vise versa, without any additional mechanism.

In order to gain a better insight into the properties of the QD spectrum, let us consider two limiting cases: (a) $\gamma k_q(E_q^n) \gg |t_m + s\lambda_x|$; and (b) $\gamma k_q(E_q^n) \ll |t_m + s\lambda_x|$. In case (a), with the aid of equation (52) we have:

$$\gamma k_q(E_q^n) \approx |E_q^n - V_0| \gg t_m + s\lambda_x, \quad z_q(E_q^n) \approx \pm i. \tag{56}$$

As a result, equation (54) transforms to the form

$$\exp\left(2i\frac{|E_q^n - V_0|}{\gamma}L\right) \approx \left(\frac{\pm i\tilde{z}_q(E_q^n) - 1}{\pm i - \tilde{z}_q(E_q^n)}\right)^2 \approx \text{const}. \tag{57}$$

At the condition $E_q^{n+1} - E_q^n \ll V_0$ it yields an equidistant spectrum similar to the one of the harmonic oscillator potential:

$$E_q^{n+1} - E_q^n \approx \frac{\gamma\pi}{L}. \tag{58}$$

In case (b), at small $k_q(E_q^n)$ we obtain

$$\gamma k_q^n(E_q^n) = \sqrt{(E_q^n - V_0)^2 - (t_m + s\lambda_x)^2} \ll t_m + s\lambda_x,$$
$$z_q(E_q^n) \approx \pm 1. \tag{59}$$

As a result, equation (54) takes the form

$$\exp\left(2ik_q^n(E_q^n)L\right) \approx 1. \tag{60}$$

At the condition $E_q^{n+1} - E_q^n \ll t_m + s\lambda_x$ it defines the spectrum similar to the one of the quantum well potential:

$$E_q^{n+1} - E_q^n \approx \left(\frac{\gamma\pi}{L}\right)^2 \frac{2n+1}{2(t_m + s\lambda_x)}. \tag{61}$$

Both limits (low-and high-energies) should be fulfilled for long nanotubes.

5 General case

5.1 Scattering on a potential step

Analytical solutions of the eigenvalue problem for the Hamiltonian (17) with nonzero λ_x and λ_y are presented in Appendix. With the aid of these results we reconsider the scattering at the interface introduced by a potential step of the height V_0 (Fig. 3). Unfortunately, analytical expressions for the general case are too cumbersome, and we present mostly numerical results. We use the same typical values for graphene nanotubes (as in the previous section) to demonstrate a general tendency.

The expectation value of the orbital (θ) current component (see Appendix, Eq. (A.7))

$$\langle\hat{j}_\theta\rangle_{m,s} = \frac{\gamma t_m}{E}\left(1 + s\frac{\lambda_x^2}{\sqrt{\lambda_x^2(t_m^2 + \lambda_y^2) + t_y^2\lambda_y^2}}\right) \tag{62}$$

essentially depends on the spin-orbit term $\lambda_y \neq 0$, ignored in literature (see Fig. 7).

The orbital current becomes zero at

$$|m| = 1/2,\ s = -1, |t_y| = \frac{\lambda_x}{\lambda_y}\sqrt{\lambda_x^2 - \lambda_y^2 - t_m^2}, \tag{63}$$

which corresponds to the energy $E = \pm 1.199$ eV for the parameters listed in the caption of Figure 2. To avoid the additional back scattering due to non-normal incidence of electrons on the potential step, we use this energy and the quantum number $m = 1/2$ for incoming electron to trace the transmission and reflection events as a function of V_0 (Fig. 8).

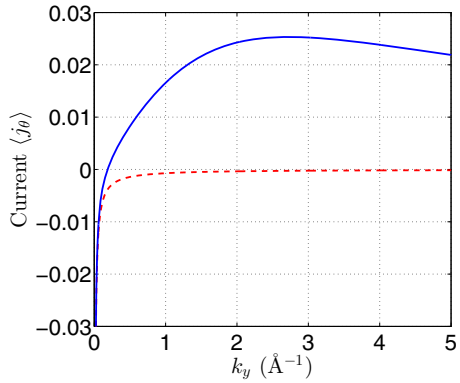

Fig. 7. Current $\langle\hat{j}_\theta\rangle_q$ (see Eq. (62)) as a function of the wave number k_y for the eigenstate with $q = \{m = 1/2, s = -1\}$ at $\lambda_x \neq 0$ for: $\lambda_y \neq 0$ (solid line) and $\lambda_y = 0$ (dashed line). The other parameters are the same as in Figure 2. At $k_y \approx 0.19$ Å $^{-1}$ the current is zero.

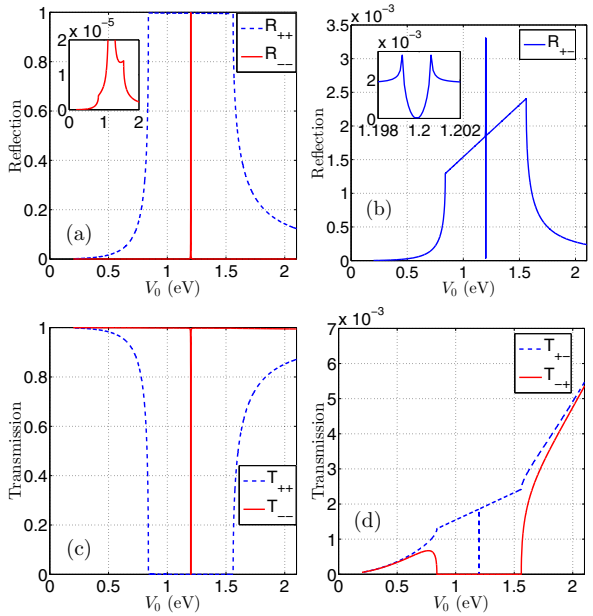

Fig. 8. Dependence of reflection (a), (b) and transmission (c), (d) probabilities for normal incidence at $m = 1/2$, $E_F = 1.199$ eV on the height of the potential step V_0 (eV). The parameters are the same as in Figure 2.

For energies $E - V_0 \leq 0.5$ eV the conductance

$$G = \frac{e^2}{h}\left(\left|t_{m,+1}^{m,+1}\right|^2 + \left|t_{m,-1}^{m,-1}\right|^2 + \left|t_{m,-1}^{m,+1}\right|^2 + \left|t_{m,+1}^{m,-1}\right|^2\right) \tag{64}$$

is dominated by the transmission without spin-flip (see Figs. 8a, 8c), i.e., by the probabilities $T_{++} = |t_{m,+1}^{m,+1}|^2$ and $T_{--} = |t_{m,-1}^{m,-1}|^2$, while the reflection is suppressed. At $E - V_0 > 0.5$ eV the SOC gives rise to the direct reflection $R_{++} = |r_{m,+1}^{m,+1}|^2$ (without spin-flip), which grows rather rapidly. Within the energy gap $-E_{m,+1}^0 < E_F - V_0 < -E_{m,-1}^0$ and $E_{m,-1}^0 < E_F - V_0 < E_{m,+1}^0$ ($E_{1/2,+1}^0 \approx 0.36$ eV) the transmission probability $T_{--} \approx 1$, while

the transmission probability T_{++} is almost suppressed, since the reflection probability $R_{++} \approx 1$. Although the probability T_{--} is a dominant process, the probability $T_{+-} = |t^{m,+1}_{m,-1}|^2$ produces a parasitic loss of this dominance due to λ_y term in the SOC. Note that the transmission probability $T_{-+} = |t^{m,-1}_{m,+1}|^2$ is completely suppressed in this energy window.

This mechanism resembles in appearance to the one considered for one-dimensional electron system formed in semiconductor heterostructures showing strong Rashba spin-orbit interaction in the presence of weak magnetic field [21]. In our case, the spin-filter effect is brought about by a relatively weak curvature-induced SOC which creates the "effective magnetic field". It is noteworthy that at $\lambda_y = 0$ the filter would be even more efficient due to the absence of the inter-channel scattering.

There is a full reflection zone which corresponds to the SOC's induced gap of the width $\Delta E_{1/2,-1} = 2\times 0.7$ meV $\approx$ 16 K for chosen parameters. In this energy interval the evanescent modes exist only. In contrast to the case considered in the previous section ($\lambda_y = 0$), there is a mixing of spin components. In general, the back scattering

$$G_{bs} = \frac{e^2}{h}\left(|r^{m,+1}_{m,+1}|^2 + |r^{m,-1}_{m,-1}|^2 + |r^{m,+1}_{m,-1}|^2 + |r^{m,-1}_{m,+1}|^2\right) \tag{65}$$

being small increases on two order in magnitude in the presence of the SOC induced by λ_y term (compare the inserts on Figs. 8a, 8b). For completeness, we consider reflection for $q_n = \{m = \pm\frac{1}{2}, s = \mp 1\}$, which corresponds to a normal incidence for the CNT without the SOC. The expansion of reflection amplitudes over the parameter δ, which is responsible for the *intrinsic* graphene spin-orbit interaction, leads to the results

$$r^{m,s}_{m,s} = \delta p \frac{\gamma}{R}\frac{V_0}{E_{in}E_{out}} + O(\delta^2), \tag{66}$$

$$r^{m,s}_{m,-s} = \frac{\lambda_y}{2t_m^2}V_0\left[\left(E_{in}^2 - 4t_m^2\right)\left(E_{in} - 2|t_m|\right)^2\right]^{1/4} \times \mathcal{Z}_1/\mathcal{Z}_2 + O\left(\delta^2\right), \tag{67}$$

$$\mathcal{Z}_1 = \mathrm{sign}\left(E_{out}\right)\sqrt{E_{out}^2 - 4t_m^2} - \left(E_{out} - 2|t_m|\right), \tag{68}$$

$$\mathcal{Z}_2 = \left(E_{out} - 2|t_m|\right)\sqrt{E_{in}^2 - 4t_m^2} + \mathrm{sign}\left(E_{in}\right) \times \mathrm{sign}\left(E_{out}\right)\left(E_{in} - 2|t_m|\right)\sqrt{E_{out}^2 - 4t_m^2}. \tag{69}$$

Here, we use the following notations: $E_{in} = E_F, E_{out} = E_F - V_0$, omitting unimportant phase factors. The direct reflection amplitude (66) is described in the lowest order by the same formula (47) as for the case $\lambda_y = 0$. Indeed, the term λ_y contributes to the direct scattering only in the second order with respect to the strength δ. Its contribution is, therefore, negligible in a direct scattering. The spin-flip reflection appears, however, due to λ_y term solely. Equations (66) and (67), reproduce remarkably well the complex behavior of reflection displayed on Figure 8b (for comparison see Fig. 4b). The reflection probabilities

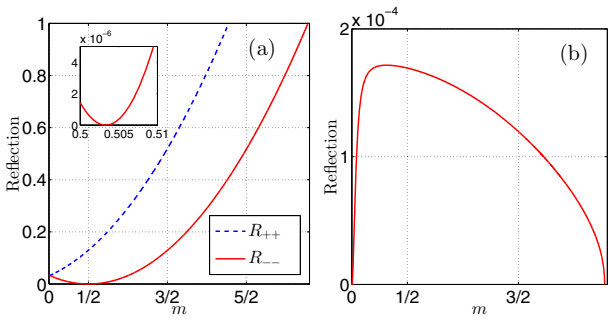

Fig. 9. Reflection probabilities as a function of the angular momentum projection m. The energy of incoming (outgoing) electron is $E_F = 1$ eV($E_F - V_0 = -1$ eV). The panel (a) displays the direct reflection probabilities: $R_{--} = |r^{m,-1}_{m,1}|^2$ (solid, red) and $R_{++} = |r^{m,+1}_{m,+1}|^2$ (dashed, blue). The panel (b) displays the reflection probabilities with the spin-flip: $R_{-+} = |r^{m,-1}_{m,+1}|^2 = |r^{m,+1}_{m,-1}|^2$. The parameters are the same as in Figure 2.

for different m are displayed on Figure 9. The direct reflection (without the spin-flip) grows rapidly with the increase of the magnetic quantum number m (see Fig. 9a). In contrast, the spin-flip reflection probabilities tends to zero with the increase of the magnetic quantum number (see Fig. 9b). In comparison with the case $\lambda_y = 0$, the minimum in the reflection probability $|r^{m,-1}_{m,-1}|^2$ is slightly shifted from $m' = 1/2 + 2p\delta$ (see the insert in Fig. 9a). In contrast to the case with $\lambda_y = 0$, the direct reflection probability $|r^{m,-1}_{m,-1}|^2$ cannot be turned to zero by the Aharonov-Bohm magnetic flux alone, created by the magnetic field along the nanotube symmetry (y-) axis. The larger is the quantum number m the smaller is the transmission probability.

The maximal magnetic quantum number m which corresponds to a complete reflection could be determined from the condition that the longitudinal current $\langle\hat{j}_y\rangle_{m,s} = 0$ (see Appendix). This condition requires $t_y = \gamma k_y = 0$ after the potential step. Note that the quantum number s is not conserved at $\lambda_y \neq 0$. As a result, one obtains with the aid of equation (A.4) for the energy of outgoing electron the condition

$$t_y = 0 \Rightarrow |E_F - V_0| = E^0_{m,s} \equiv |E_{m,s}(k_y = 0)|, \tag{70}$$

$$E_{m,s}(k_y = 0) = \sqrt{t_m^2 + \lambda_y^2} + s\lambda_x, \quad s = \pm 1. \tag{71}$$

At fixed parameters $\{E_F, V_0, \lambda_{x,y}, R\}$, one defines the boundaries

$$C_\pm = t_m^2 = \left(\frac{\gamma}{R}m\right)^2 = \left(|E_F - V_0| \mp \lambda_x\right)^2 - \lambda_y^2. \tag{72}$$

Note that $C_- > C_+$, and, therefore, the maximal $m = M$ is determined as:

$$M = \frac{R}{\gamma}\sqrt{C_-}. \tag{73}$$

For all $|m| \geq M$ the transmition probability $T_{s-} \equiv 0$ for $s = \pm 1$. In particular, for our choice of parameters the

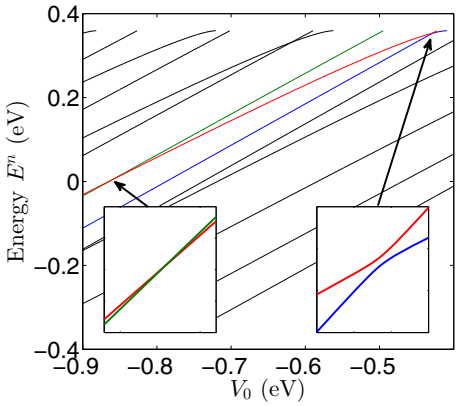

Fig. 10. The QD energy spectrum as a function of applied potential V_0. The levels with a quantum number $m = 3/2$ are displayed for the nanotube with a length $L = 100$ Å. The other parameters are the same as in Figure 2. At different values of the applied potential, levels either cross (left insert) or repel (right insert) each other.

reflection probability $R_{--} = |r^{m,-1}_{m,-1}|^2 = 1$ at $M \approx 7/2$ (compare with Fig. 9a).

From now on we can define the critical angle of the complete reflection. In virtue of results from Appendix we obtain for the critical angle

$$\tan(\phi) = \frac{\langle j_\theta \rangle_q}{\langle j_y \rangle_q} = \frac{t_M}{t_y}\left(1 + \frac{\lambda_x^2 - \lambda_y^2}{W}\right), \qquad (74)$$

$$W = \sqrt{\lambda_y^2 E_F^2 + t_M^2(\lambda_x^2 - \lambda_y^2)}, \qquad (75)$$

where the critical value of the magnetic quantum number m is related to the variable t_M

$$t_M = \sqrt{C_-} = \sqrt{(|E_F - V_0| + \lambda_x)^2 - \lambda_y^2}. \qquad (76)$$

We use $s = +1$ in equation (74), since $t_y(s = +1) < t_y(s = -1)$, where t_y is defined by equation (A.8)

$$t_y = \gamma k_s = \sqrt{E_F^2 + \lambda_y^2 - t_M^2 - \lambda_x^2 - 2sW}. \qquad (77)$$

These equations might provide some hint on the contribution of different SOC terms at experimental measurements of the critical angle.

5.2 Basic features of quantum dot

The energy spectrum of QD is defined by the minimal gap for a given angular momentum m: $-E^0_{m,-1} < E^n_m < E^0_{m,-1}$. The mixing of spin components could lead to the interaction between spectra inherited from the ones with different spin projection for the case $\lambda_y = 0$. In particular, a crossing/anti-crossing behavior of two levels depends on their symmetry with respect to the inversion of the y-axis (see Fig. 10). Two levels with the same parity $\Psi_{1,2} = s_{1,2}\hat{M}_y\Psi_{1,2}$ (when $s_1 = s_2$) anti-cross, while a different sign $s_1 = -s_2$ leads to the level crossing. Other properties of discrete levels are very similar to properties of those obtained at $\lambda_y = 0$.

6 Summary

Within the approach suggested by Ando (see details in [11]), we solved analytically the eigenvalue problem for the effective mass Hamiltonian for electrons on curved surface with the spin-orbit interaction. In particular, with the aid of transformation (7), we obtained explicit expressions for a low energy spectrum and eigenstates of armchair carbon nanotubes. These findings have been used to analyze transport properties of CNT with curvature-induced SOC (see Eq. (11)) at different limits.

We have analyzed effects produced by the SOC on the scattering of electrons at the interface introduced by the potential step of height V_0. The effect of the SOC becomes especially drastic when the height of the potential barrier can be controlled to reach conditions allowing to produce a spin-filter effect. At this condition only one spin component is dominant in the transmission over the CNT. Note that this phenomenon occurs due to the "effective magnetic field" which is brought about by the curvature induced SOC. The SOC term λ_y yields, however, a parasite loss ($\sim 10^{-3}$) of the spin-filter effect.

The gap in CNTs (due to the SOC) opens a possibility to create a nanotube quantum dot. In the limit of the preserved spin symmetry we have calculated the QD eigenstates with the aid of the transcendental equation. At low energy limit the spectrum is similar to the one of the quantum well potential, while for large energies it carries features of the harmonic oscillator spectrum. In such QDs the electron with spin up cannot scatter into state with spin down and vise versa, without any additional mechanism. However, the SOC term λ_y mixes these states and yields the anti-crossing effect. This mechanism may affect the spin relaxation phenomenon in the system under consideration, in addition to an electron-phonon coupling mechanism [16].

There was a belief that the curvature induced SOC in graphene, restricted by the first term, leads only to very weak back scattering [11]. We have demonstrated, however, that the second term, ignored in a previous analysis, produces the inter-channel scattering, which could increase the back scattering by a few orders of magnitude and enrich transport phenomena in carbon nanotubes.

K.N.P. and M.P. are grateful for the congenial hospitality at UIB and JINR. This work was supported in part by RFBR Grant 14-02-00723, integration Grant No. 29 from the Siberian Branch of the RAS and Slovak Grant Agency VEGA Grant No. 2/0037/13.

Appendix: An eigenvalue problem for $\hat{H}'$

We suggest to use the eigenstate in the form

$$F'(\theta, y) = e^{im\theta}e^{ik_y y}\begin{pmatrix} A \\ B \\ C \\ D \end{pmatrix}, \quad m = \pm 1/2, \pm 3/2, \ldots \quad (A.1)$$

to solve the eigenvalue problem $\hat{H}'F' = EF'$ for the Hamiltonian (8). As a result, one obtains the Hamiltonian (17). In virtue of the unitary transformation

$$\begin{aligned}\tilde{V} &= \hat{P}_{123}\hat{\tau}_x \otimes \exp\left(i\frac{\pi}{4}\hat{\sigma}_x\right)\\ &= \frac{1}{\sqrt{2}}\begin{pmatrix}0&0&1&0\\1&0&0&0\\0&1&0&0\\0&0&0&1\end{pmatrix}\begin{pmatrix}0&0&1&i\\0&0&i&1\\1&i&0&0\\i&1&0&0\end{pmatrix}\\ &= \frac{1}{\sqrt{2}}\begin{pmatrix}1&i&0&0\\0&0&1&i\\0&0&i&1\\i&1&0&0\end{pmatrix}\end{aligned} \tag{A.2}$$

our Hamiltonian (17) becomes real

$$\begin{aligned}\hat{\tilde{H}} &= \tilde{V}^{-1}\hat{H}'\tilde{V}\\ &= \begin{pmatrix}-\lambda_x-\lambda_y & 0 & t_y & t_m\\ 0 & \lambda_x+\lambda_y & t_m & -t_y\\ t_y & t_m & \lambda_x-\lambda_y & 0\\ t_m & -t_y & 0 & -\lambda_x+\lambda_y\end{pmatrix}\end{aligned} \tag{A.3}$$

with notations (18). The eigenvalues of the Hamiltonian (A.3) are

$$\begin{aligned}E &= \pm E_{m,s},\\ E_{m,s} &= \sqrt{t_m^2+t_y^2+\lambda_y^2+\lambda_x^2+2D_{m,s}}, \quad s=\pm 1,\\ D_{m,s} &= s\sqrt{\lambda_x^2\left(t_m^2+\lambda_y^2\right)+t_y^2\lambda_y^2}.\end{aligned} \tag{A.4}$$

Eigenvectors have rather simple form

$$\begin{aligned}\mathcal{V}_{m,s} = \frac{1}{N_{m,s}}\Bigg(&\frac{-D_{m,s}+\lambda_y(E-\lambda_y)}{t_m(\lambda_x+\lambda_y)},\\ &\frac{-t_y(\lambda_x-\lambda_y)}{-D_{m,s}+\lambda_x(E-\lambda_x)}, \frac{t_y}{t_m}\frac{(-D_{m,s}+\lambda_y(E-\lambda_y))}{(-D_{m,s}+\lambda_x(E-\lambda_x))}, 1\Bigg)^T,\end{aligned} \tag{A.5}$$

where the values $E = \pm E_{m,s}$, $D_{m,s}$ are defined by equation (A.4), and the norm $N_{m,s}$ is:

$$\begin{aligned}N_{m,s} &= \sqrt{(\mathcal{F}_1+\mathcal{F}_2+\mathcal{F}_3)/\mathcal{M}+1},\\ \mathcal{F}_1 &= \left(D_{m,s}-\lambda_y(E-\lambda_y)\right)^2\left(D_{m,s}-\lambda_x(E-\lambda_x)\right)^2,\\ \mathcal{F}_2 &= t_m^2t_y^2(\lambda_x^2-\lambda_y^2)^2,\\ \mathcal{F}_3 &= t_y^2(\lambda_x+\lambda_y)^2\left(D_{m,s}-\lambda_y(E-\lambda_y)\right)^2,\\ \mathcal{M} &= t_m^2(\lambda_x+\lambda_y)^2(D_{m,s}-\lambda_x(E-\lambda_x))^2.\end{aligned} \tag{A.6}$$

The expectation value of the current for eigenspinors (A.5) could be calculated with the aid of the definitions (27) and the transformation (A.2). As a result, we obtain

$$\begin{aligned}\langle\hat{j}_y\rangle_{m,s} &= \frac{\gamma t_y}{E}\left(1+\frac{\lambda_y^2}{D_{m,s}}\right),\\ \langle\hat{j}_\theta\rangle_{m,s} &= \frac{\gamma t_m}{E}\left(1+\frac{\lambda_x^2}{D_{m,s}}\right).\end{aligned} \tag{A.7}$$

To solve a scattering problem we need the eigenspinors for a fixed value of the energy E. Using the dispersion relation (A.4), we obtain

$$k_{m,s} = \frac{1}{\gamma}\sqrt{E^2+\lambda_y^2-t_m^2-\lambda_x^2-2s\sqrt{\lambda_y^2E^2+t_m^2\left(\lambda_x^2-\lambda_y^2\right)}}. \tag{A.8}$$

Substituting the value of $k_{m,s}$ from equation (A.8), the spinor (A.5) becomes $\mathcal{V}_{m,s}(t_y = \gamma k_{m,s})$ with the parameter $D_{m,s}$ simplified to the form

$$D_{m,s} = s\sqrt{\lambda_y^2E^2+t_m^2(\lambda_x^2-\lambda_y^2)}-\lambda_y^2. \tag{A.9}$$

References

1. R. Saito, G. Dresselhaus, M.S. Dresselhaus, *Physical Properties of Carbon Nanotubes* (Imperial College Press, London, 1998)
2. T. Ando, J. Phys. Soc. Jpn **74**, 777 (2005)
3. M.S. Dresselhaus, G. Dresselhaus, R. Saito, A. Jorio, Phys. Rep. **409**, 47 (2005)
4. J.-C. Charlier, X. Blase, S. Roshe, Rev. Mod. Phys. **79**, 677 (2007)
5. Q. Zhang, J-Qi Huang, W.-Z. Qian, Y.-Y. Zhang, F. Wei, Small **8**, 1237 (2013)
6. S.W. Lee, E.E.B. Campbell, Curr. Appl. Phys. **13**, 1844 (2013)
7. H. Min, J.E. Hill, N.A. Sinitsyn, B.R. Sahu, L. Kleinman, A.H. MacDonald, Phys. Rev. B **74**, 165310 (2006)
8. A.H. Castro Neto, F. Guinea, N.M.R. Peres, K.S. Novoselov, A.K. Geim, Rev. Mod. Phys. **81**, 109 (2009)
9. C.L. Kane, E.J. Mele, Phys. Rev. Lett. **78**, 1932 (1997)
10. P. Allain, J. Fuchs, Eur. Phys. J. B **83**, 301 (2011)
11. T. Ando, J. Phys. Soc. Jpn **69**, 1757 (2000)
12. M.V. Entin, L.I. Magarill, Phys. Rev. B **64**, 085330 (2001)
13. A. De Martino, R. Egger, K. Hallberg, C.A. Balseiro, Phys. Rev. Lett. **88**, 206402 (2002)
14. D. Huertas-Hernando, F. Guinea, A. Brataas, Phys. Rev. B **74**, 155426 (2006)
15. F. Kuemmeth, S. Ilani, D.C. Ralph, P.L. McEuen, Nature **452**, 448 (2008)
16. D.V. Bulaev, B. Trauzettel, D. Loss, Phys. Rev. B **77**, 235301 (2008)
17. L. Chico, M.P. López-Sancho, M.C. Muñoz, Phys. Rev. B **79**, 235423 (2009)
18. J.-S. Jeong, H.-W. Lee, Phys. Rev. B **80**, 075409 (2009)
19. W. Izumida, K. Sato, R. Saito, J. Phys. Soc. Jpn **78**, 074707 (2009)
20. M. del Valle, M. Magrańska, M. Grifoni, Phys. Rev. B **84**, 165427 (2011)
21. P. Středa, P. Šeba, Phys. Rev. Lett. **90**, 256601 (2003)